IEEE Access
Multidisciplinary ⋮ Rapid Review ⋮ Open Access Journal

Received 11 March 2023, accepted 1 May 2023, date of publication 5 May 2023, date of current version 10 May 2023.

Digital Object Identifier 10.1109/ACCESS.2023.3273296

RESEARCH ARTICLE

A Robust Method for Block Adjustment of UAV SAR Images

YUNHAO CHANG[1,2], QING XU[1], XIN XIONG[1], GUOWANG JIN[1], HUITAI HOU[1], AND RUIBING CUI[1,2]

[1]Institute of Geospatial Information, Information Engineering University, Zhengzhou, Henan 450001, China
[2]Henan College of Surveying and Mapping, Zhengzhou, Henan 450000, China

Corresponding author: Qing Xu (13937169139@139.com)

This work was supported in part by the National Natural Science Foundation of China under Grant 41474010 and Grant 42201492, and in part by the Wisdom Central Plains Geographic Information Technology Henan Provincial Collaborative Innovation Center Spatiotemporal Perception and Intelligent Processing Ministry of Natural Resources Key Laboratory Joint Fund under Grant 212109.

ABSTRACT To reduce the number of ground control points required for block adjustment of unmanned aerial vehicle (UAV) synthetic aperture radar (SAR) images, a robust block adjustment method is pro-posed. The proposed method aims to solve the problem of unstable adjustment solutions caused by the jittering of UAV SAR platforms. This method is based on the range Doppler model. By analyzing the correlation between the antenna phase center, velocity, and Doppler centroid of the seven orientation parameters, this method performs a block adjustment of UAV SAR images with three orientation parameters: the antenna phase center initial imaging moment, Doppler centroid, and proximity delay. UAV SAR images obtained from an area of 2×3 km in Dengfeng were used to conduct adjustment experiments. The results obtained using different orientation parameter set-tings verify the robustness and effectiveness of the proposed method. The adjustment results under various control-point layout plans indicate that a uniform layout plan can achieve an adjustment accuracy better than 1 m with a small number of control points.

INDEX TERMS Unmanned aerial vehicle (UAV), SAR images, range Doppler model, three-parameter, block adjustment.

I. INTRODUCTION

Unmanned aerial vehicle (UAV) synthetic aperture radar (SAR) is a new surveying and mapping system, which includes a combination of SAR sensors on a UAV platform. The system exploits the features of targeted data acquisition, short cycle time, low cost, safety and reliability, mobility, and flexibility enabled by the UAV platform, as well as the active all-day microwave remote sensing and all-weather acquisition of high-resolution images offered by the SAR sensor [1], [2]. UAV SAR has been widely used in topographic surveying [3], emergency surveying [4], landslide detection [5], forest monitoring [6], and other fields. To conduct topographic surveys using a UAV SAR system and generate high-resolution images, the orientation parameters of each SAR image must be accurately acquired using block adjustment with the support of ground control points [7]. However, due to the low flight altitude and small imaging width of the UAV SAR, multiple images of multiple strips are required to cover the entire survey area. Thus, a large number of control points are required for block adjustment to obtain the orientation parameters. In addition, the vibration of the UAV SAR leads to a lack of robustness in the block-adjustment solution. To reduce the number of control points required for adjust-ment, enhance the robustness of the adjustment solution, and to improve the effectiveness and performance of surveying and producing UAV SAR images, obtaining a robust solution for block adjustment is an urgent requirement.

The first step in achieving block adjustment of the SAR images is to select a suitable imaging model. Common imaging models include range-Doppler (RD) [8], range

The associate editor coordinating the review of this manuscript and approving it for publication was Halil Ersin Soken.

co-planarity [9], equivalent collinearity [10], and rational function models (RFM) [11]; specifically, the RD model is also known as the Leberl model under the zero Doppler effect [12]. Considerable research has been conducted on block-adjustment methods based on the aforementioned imaging models. Xiong et al. [7] solved seven orientation parameters of the RD model in a UAV SAR image area using a route-constraint model. Yue et al. [13] explored a block adjustment algorithm for UAV SAR images based on the Leberl and RD models under sparse or no control conditions. Zhang et al. [14] derived an unbiased estimation of the rational polynomial coefficient (RPC) for SAR images by analyzing the geometric effect of SAR images, and demonstrated that the RPC model is applicable to satellite SAR images using a large number of strict sensor-based experiments. Jiao et al. [15] proposed an error source-based method to improve the geometric positioning accu-racy of Gaofen-3 (GF-3) SAR satellites. Zhang et al. [16] used the RD model to construct a position and orientation system (POS) to assist the aerotriangulation model for UAV SAR images. In addition, Jiao et al. [17] proposed a new slant-range error update model and an error-source-based weighting strategy that can effectively improve the three-dimensional (3D) geolocation accuracy of the multi-observation dataset of GF-3 satellites. Yang et al. [18] matched SAR images with data from imaging models and information from an ex-ternal digital elevation model (DEM) to perform block adjustment. Toutin and Omari [19] created a new hybrid model by combining RFM and physical models to process RADAR-SAT-2 data without ground control points. Huang and He [20] combined model construction, parameter solutions, and RFM model refinement for block adjustment. Zhang et al. [21] generated an RPC model by compensating GF-3 satellite images with geometric calibration and then used a digital elevation model (DEM) to assist block adjustment. Jiao et al. [22] used the OS-SIFT algorithm [23] to match the optical and SAR images and performed joint adjustment with the RFM model.

Current studies on block adjustment mainly focus on satellite-and large air-craft-based SAR images. Except for the study conducted by Xiong et al. [7], in which UAV SAR images were incorporated into the experiments, there have been few studies on UAV SAR images. Compared to satellite-and large aircraft-based SAR systems, the UAV SAR system has a smaller imaging width and poorer platform stability. In response to these features, this study presents the design of a block adjustment method for UAV SAR images that solves three orientation parameters: the initial imaging moment of the antenna phase center, Doppler centroid, and proximity delay, which effectively improves the robustness and accuracy of the adjustment solution.

The contributions of the work are as follows.

1. A robust block adjustment algorithm based on RD model for UAV SAR image is proposed.
2. The influence of the number and distribution of different control points on the adjustment results is analyzed.

The remainder of this paper is organized as follows. The basic RD model and our proposed selection of orientation parameters are introduced in Sec. II. In Sec. III, the experimental results are presented to verify the robustness and accuracy of our proposed block adjustment method using SAR images covering the Dengfeng area. Finally, the conclusions and discussion are presented in Sec. IV.

II. ROBUST APPROACH TO BLOCK ADJUSTMENT OF UAV SAR IMAGES

A. RANGE DOPPLER MODEL

The RD model is a direct description of the SAR imaging principle [24] and has clear geometric and physical meanings [25]. The model uses the distance and Doppler condition equations to describe the correspondence between the ground point and corresponding image point at a given moment as follows:

$$\begin{gathered} R_S^2 = (R_0 + M_s \cdot x)^2 = (X - X_S)^2 + (Y - Y_S)^2 + (Z - Z_S)^2 \\ V_X\,(X - X_S) + V_Y\,(Y - Y_S) + V_Z\,(Z - Z_S) = -\frac{\lambda R_S}{2} f_{dc} \end{gathered} \tag{1}$$

where (X, Y, Z) represent the coordinates of the ground point in the object space coordinate system; (x, y) represent the pixel coordinates of the image point; x represents the range; y represents the azimuth; $\left[X_S\ Y_S\ Z_S\right]^T$ is the instantaneous position vector of the antenna phase center; M_s is the slant range sampling interval; R_0 is the proximity delay; f_{dc} is the Doppler shift parameter; $\left[V_X\ V_Y\ V_Z\right]^T$ is the instantaneous velocity vector of the time-of-flight; and λ is the radar wavelength. The antenna phase center and flight velocity were calculated as follows:

$$\begin{cases} t = t' \cdot y + t_0 \\ X_S = X_{S_0} + V_{X_0} \cdot t + a_{X_0} \cdot t^2 + \cdots \\ Y_S = Y_{S_0} + V_{Y_0} \cdot t + a_{Y_0} \cdot t^2 + \cdots \\ Z_S = Z_{S_0} + V_{Z_0} \cdot t + a_{Z_0} \cdot t^2 + \cdots \\ V_X = V_{X_0} + 2a_{X_0} \cdot t + \cdots \\ V_Y = V_{Y_0} + 2a_{Y_0} \cdot t + \cdots \\ V_Z = V_{Z_0} + 2a_{Z_0} \cdot t + \cdots \end{cases} \tag{2}$$

where t' is the temporal interval between adjacent azimuthal rows; typically, the ratio of the azimuthal distance and sampling interval M_a; t_0 is the imaging moment of the first-row images, $\left[a_{X_0}\ a_{Y_0}\ a_{Z_0}\right]^T$ is the antenna phase center acceleration vector at the initial moment, $\left[V_{X_0}\ V_{Y_0}\ V_{Z_0}\right]^T$ is the time-of-flight instantaneous velocity vector at the initial moment, and $\left[X_{S_0}\ Y_{S_0}\ Z_{S_0}\right]^T$ is the antenna phase center instantaneous position vector at the initial moment.

B. SELECTION OF ORIENTATION PARAMETERS

Seven parameters, namely, the initial position of the antenna phase center $\left[X_{S_0}\ Y_{S_0}\ Z_{S_0}\right]^T$, initial velocity $\left[V_{X_0}\ V_{Y_0}\ V_{Z_0}\right]^T$, and Doppler centroid f_{dc}, are generally selected as the orientation parameters for block adjustment of

SAR images using the RD model [7]. The seven-parameter method can efficiently restore the motion state of the SAR system and is suitable for the block-adjustment solution of both satellite-based and airborne SAR images. However, UAV SAR images have a smaller width, and a large number of SAR images are required to cover the survey area. The need for additional parameters for the adjustment solution will require a large number of ground control points, resulting in slow convergence or even non-convergence of the adjustment solution. Given that the initial velocity and Doppler centroid have a certain degree of correlation and that the velocity data from the POS data are generally relatively accurate, a total of four parameters, namely, the initial velocity of the antenna phase center $\left[X_{S_0} \ Y_{S_0} \ Z_{S_0} \right]^T$ and the Doppler centroid f_{dc}, can be selected as the orientation parameters [26]. In comparison with the seven-parameter method, the four-parameter method reduces the correlation between the orientation parameters and improves robustness and efficiency. However, the UAV SAR platforms has poor flight stability. Thus, during the adjustment solution, the errors in the initial position are inclined to compensate for each other in the two directions (i.e., range and vertical direction) of the vertical flight trajectory, which is not conducive to the rapid convergence of the adjustment solution.

To address the problems related to the seven- and four-parameter methods, considering the features of the UAV SAR platform, this study selected the three orientation parameters for the block-adjustment solution: the initial imaging moment of the antenna phase center t_0, Doppler shift parameter f_{dc}, and proximity delay R_0. The three-parameter method restricts the initial position error to the along-the-track direction (azimuth) and the slant range direction, which avoids errors from the compensation of the range and vertical direction and reduces the correlation between the orientation parameters. This is conducive to the fast convergence of the adjustment solution and can effectively improve the robustness of the block-adjustment solution of UAV SAR images.

C. ORIENTATION PARAMETER SOLVING

After determining the orientation parameters, (2) can be simplified to

$$\begin{cases} t = t' \cdot y + t_0 \\ X_S = X_{S_0} + V_{X_0} \cdot t \\ Y_S = Y_{S_0} + V_{Y_0} \cdot t \\ Z_S = Z_{S_0} + V_{Z_0} \cdot t \\ V_X = V_{X_0} \\ V_Y = V_{Y_0} \\ V_Z = V_{Z_0} \end{cases} \tag{3}$$

The RD model is nonlinear and must be linearized to solve the orientation parameters. According to (1):

$$F_1 = (X - X_S)^2 + (Y - Y_S)^2 + (Z - Z_S)^2 - (R_0 + M_s \cdot x)^2$$

$$F_2 = V_X (X - X_S) + V_Y (Y - Y_S) + V_Z (Z - Z_S) + \frac{\lambda (R_0 + M_s \cdot x)}{2} f_{dc} \tag{4}$$

The error equation after linearization is

$$\boldsymbol{V} = \boldsymbol{A} \cdot \boldsymbol{\Delta}_P + \boldsymbol{B} \cdot \boldsymbol{\Delta}_G - \boldsymbol{L} \quad \boldsymbol{P} \tag{5}$$

where $\boldsymbol{V}$ is the error vector, $\boldsymbol{A}$ is the coefficient matrix of the orientation parameter corrections, $\boldsymbol{\Delta}_P$ is the orientation parameter correction vector, $\boldsymbol{B}$ is the coefficient matrix of the ground point coordinate corrections, $\boldsymbol{\Delta}_G$ is the ground point coordinate correction vector, $\boldsymbol{L}$ is a constant term, and $\boldsymbol{P}$ is the weight matrix.

The observations in the error equation include the range coordinate x and azimuthal coordinate y of the image point, which are considered independent of each other, and the root mean square errors (RMSE) are m_x and m_y, respectively. The unit weight RMSE is taken to be μ, and the weight matrix $\boldsymbol{P}$ of the error equation, according to the weight inverse matrix propagation formula, is

$$\boldsymbol{P} = \begin{bmatrix} \dfrac{\mu^2}{\left(\frac{\partial F_1}{\partial x}\right)^2 m_x^2 + \left(\frac{\partial F_1}{\partial y}\right)^2 m_y^2} & 0 \\ 0 & \dfrac{\mu^2}{\left(\frac{\partial F_2}{\partial x}\right)^2 m_x^2 + \left(\frac{\partial F_2}{\partial y}\right)^2 m_y^2} \end{bmatrix} \tag{6}$$

For a ground control point j, which is located at the overlap of the m images, the error equation can be formulated according to the RD model, and the unknown in the equation is the parameter correction in the m SAR images. The error equation is expressed as follows:

$$\boldsymbol{V}_{GCPj} = \boldsymbol{A}_{GCPj} \cdot \boldsymbol{\Delta}_{GCPj} - \boldsymbol{L}_{GCPj} \quad \boldsymbol{P}_{GCPj} \tag{7}$$

where $\boldsymbol{V}_{GCPj} = \left[\boldsymbol{V}_1 \ \boldsymbol{V}_2 \ \ldots \ \boldsymbol{V}_m \right]^T_{2m\times 1}$ is the residual vector, $\boldsymbol{\Delta}_{GCPj} = \left[\boldsymbol{\Delta}_{P1} \ \boldsymbol{\Delta}_{P2} \ \ldots \ \boldsymbol{\Delta}_{Pm} \right]^T_{3m\times 1}$ is the orientation parameter correction vector, $\boldsymbol{L}_{GCPj} = \left[\boldsymbol{L}_{1j} \ \boldsymbol{L}_{2j} \ \ldots \ \boldsymbol{L}_{mj} \right]^T_{2m\times 1}$ is the constant term vector, $\boldsymbol{A}_{GCPj}$ is the matrix of the orientation parameter correction coefficients of order $2m \times 3m$, and $\boldsymbol{P}_{GCPj}$ is the weight matrix of order $2m \times 2m$.

For a particular connection point k, which is located at the overlap of n images, the unknowns in the error equation contain the ground coordinate corrections of the connection point $\boldsymbol{\Delta}_{Gk}$, in addition to the RD model parameter corrections in the n SAR images. The error equation is

$$\boldsymbol{V}_{TPk} = \boldsymbol{A}_{TPk} \cdot \boldsymbol{\Delta}_{TPk} + \boldsymbol{B}_{TPk} \cdot \boldsymbol{\Delta}_{Gk} - \boldsymbol{L}_{TPk} \quad \boldsymbol{P}_{TPk} \tag{8}$$

where $\boldsymbol{V}_{TPk} = \left[\boldsymbol{V}_1 \ \boldsymbol{V}_2 \ \ldots \ \boldsymbol{V}_n \right]^T_{2n\times 1}$ is the residual vector, $\boldsymbol{\Delta}_{TPk} = \left[\boldsymbol{\Delta}_{P1} \ \boldsymbol{\Delta}_{P2} \ \ldots \ \boldsymbol{\Delta}_{Pn} \right]^T_{3n\times 1}$ is the orientation parameter correction vector, $\boldsymbol{\Delta}_{Gk}$ is the ground coordinate correction of the connection point, $\boldsymbol{L}_{TPk} = \left[\boldsymbol{L}_{1k} \ \boldsymbol{L}_{2k} \ \ldots \ \boldsymbol{L}_{nk} \right]^T_{2n\times 1}$ is the constant-term vector, $\boldsymbol{A}_{TPk}$ is the matrix of the orientation parameter correction coefficients of order $2n \times 3n$, $\boldsymbol{B}_{TPk}$ is

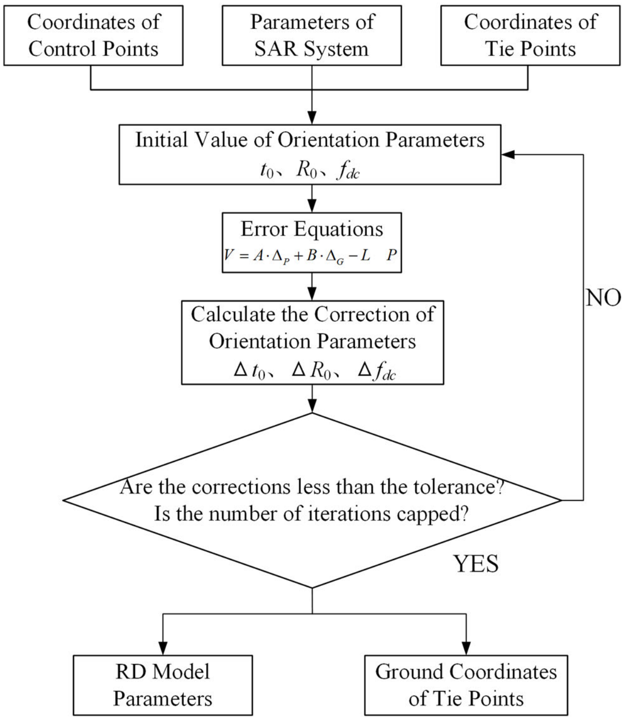

FIGURE 1. Process of the block adjustment.

the matrix of the connection point correction coefficients of order $2n \times 3$, and $\boldsymbol{P}_{TPk}$ is the weight matrix of order $2n \times 2n$.

The error equations for the control and connection points are formulated according to (7) and (8), respectively. Meanwhile, the error equation for the UAV SAR block adjustment is

$$\boldsymbol{V} = \boldsymbol{C}\cdot\boldsymbol{\Delta}_O + \boldsymbol{D}\cdot\boldsymbol{\Delta}_G - \boldsymbol{L} \quad \boldsymbol{P} \tag{9}$$

where $\boldsymbol{V}$ is the residual vector, $\boldsymbol{C}$ is the matrix of the orientation parameter correction coefficients, $\boldsymbol{\Delta}_O$ is the orientation parameter correction vector, $\boldsymbol{D}$ is the matrix of the ground coordinate correction coefficients, $\boldsymbol{\Delta}_G$ is the ground coordinate correction vector, $\boldsymbol{L}$ is a constant term vector, and $\boldsymbol{P}$ is the weight matrix. We have

$$\begin{aligned} \boldsymbol{C} &= \begin{bmatrix} \boldsymbol{A}_{GCP} \\ \boldsymbol{A}_{TP} \end{bmatrix} \quad \boldsymbol{D} = \begin{bmatrix} 0 \\ \boldsymbol{B}_{TP} \end{bmatrix} \\ \boldsymbol{L} &= \begin{bmatrix} \boldsymbol{L}_{GCP} \\ \boldsymbol{L}_{TP} \end{bmatrix} \quad \boldsymbol{P} = \begin{bmatrix} \boldsymbol{P}_{GCP} & 0 \\ 0 & \boldsymbol{P}_{TP} \end{bmatrix} \end{aligned} \tag{10}$$

The corresponding normal equation is

$$\begin{bmatrix} \boldsymbol{C}^T\boldsymbol{PC} & \boldsymbol{C}^T\boldsymbol{PD} \\ \boldsymbol{D}^T\boldsymbol{PC} & \boldsymbol{D}^T\boldsymbol{PD} \end{bmatrix} \begin{bmatrix} \boldsymbol{\Delta}_O \\ \boldsymbol{\Delta}_G \end{bmatrix} = \begin{bmatrix} \boldsymbol{C}^T\boldsymbol{PL} \\ \boldsymbol{D}^T\boldsymbol{PL} \end{bmatrix} \tag{11}$$

An iterative solution of the normal equations yields the RD model orientation parameters and the ground coordinates of the connection points for each SAR image.

The process for solving the SAR image block adjustment is presented in Fig. 1.

The following is the process for solving the SAR image block adjustment:

1. The ground and image coordinates of the control point, image coordinates of the connection point, and SAR system parameters are obtained. The SAR system parameters include the slope range sampling interval M_s, azimuth sampling interval M_a, radar wavelength λ, instantaneous position vector of the antenna phase center at the initial moment $\begin{bmatrix} X_{S_0} & Y_{S_0} & Z_{S_0} \end{bmatrix}^T$, and instantaneous velocity vector at the initial moment $\begin{bmatrix} V_{X_0} & V_{Y_0} & V_{Z_0} \end{bmatrix}^T$.
2. The ground coordinates of the connection point and initial values of the orientation parameters were determined. The orientation parameters included the initial imaging moment, t_0, Doppler shift parameter f_{dc}, and proximity delay R_0.
3. The error and normal equations are formulated to solve the corrections of the SAR image orientation parameter t_0, f_{dc}, R_0, and the ground coordinates of the connection point (X, Y, Z). Subsequently, the initial values are corrected using the solved corrections.
4. Steps 2 and 3 are repeated until all corrections satisfy the given conditions for convergence or until the preset upper limit of the number of iterations is reached. Finally, the orientation parameters and ground coordinates of the connection points of all SAR images are obtained.

III. EXPERIMENTAL RESULTS AND ANALYSIS

A. EXPERIMENTAL DATA

To verify the effectiveness of the proposed method, we selected the UAV SAR images of the Dengfeng area in Henan Province acquired in March 2022 to conduct the block adjustment experiment. The airborne platform used for data acquisition was the Zongheng CW-30 medium-sized vertical takeoff and landing (VTOL) fixed-wing UAV loaded with MicroSAR sensors developed by the Institute of Electronics, Chinese Academy of Sciences. The sensor features a right-side averted vision as the imaging mode, and the operating frequency band is Ku-band. The experimental area is approximately 2 km from east to west and 3 km from north to south. It mainly consists of plains and hills, including residential areas, water systems, roads, vegetation, and other surface features. The highest elevation in the area is approximately 562 m, and it is located in the southwestern hilly region. The lowest elevation is approximately 424 m and is located southeast of the reservoir. The scope of the survey and topographic information are presented in Fig. 2.

The relative altitude of the flight was approximately 600 m, and the direction was from west to east, with a total of 13 strips. Specifically, 2–3 images were acquired for each strip, with an overlap of approximately 60% between the images of the adjacent strips (Fig. 3).

A total of 28 SAR images were acquired in the experimental area, and Table 1 lists the basic parameters.

Two example images of adjacent strips are shown in Fig. 4. Here, the horizontal to the right is the azimuthal direction, and the vertical down is the range direction.

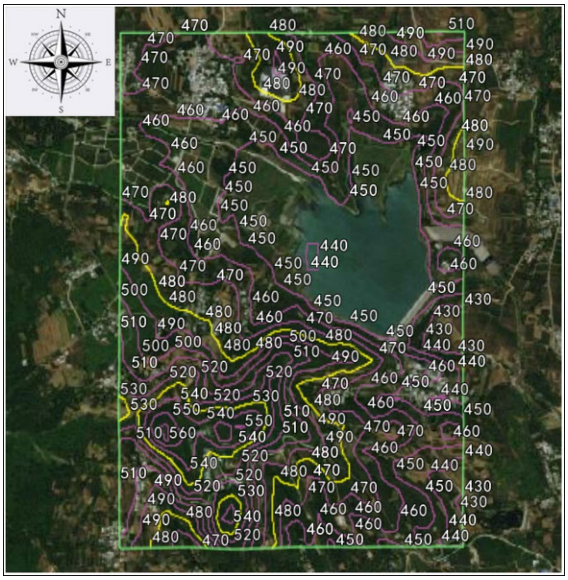

FIGURE 2. Experimental area coverage and terrain information.

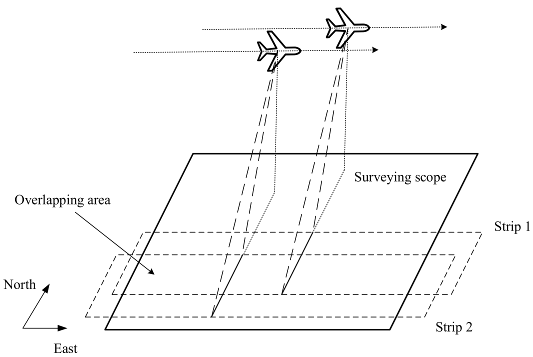

FIGURE 3. UAV SAR stereo imaging.

TABLE 1. Basic parameters of SAR images.

Parameters	Numerical value
Frequency band	Ku
Radar wavelength (mm)	20.534
Number of range direction pixels	3328
Number of azimuthal direction pixels	16384
Range direction sampling interval (m)	0.0539
Azimuthal direction sampling interval (m)	0.1249

Block adjustment of UAV SAR images requires a certain number of ground control points to be acquired, and a certain number of checkpoints are required to verify the adjustment accuracy. In this study, 9 control points were obtained by field measurements using corner reflectors, and 52 control points were manually collected using high-precision optical digital orthophoto maps (DOM) and digital surface models (DSM) of the area. The corner reflectors are mainly located in flat and open areas, and the manually selected points are mainly obvious markers (e.g., house corners, road intersections, and street light bases), as control points cannot be selected in dense vegetation and water areas. The coordinates of the corner reflector were obtained using real-time kinematics (RTK) with a point accuracy of 2–3 cm. For the points selected using high-precision optical DOM and DSM, the point accuracy was approximately 4.7 cm. The accuracy of both types of control points was in accordance with relevant standards. Some of the control points are presented in Fig. 5.

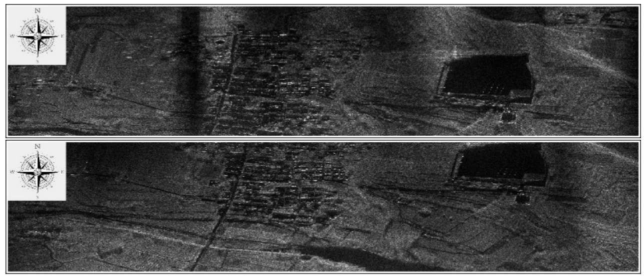

FIGURE 4. Examples of UAV SAR images.

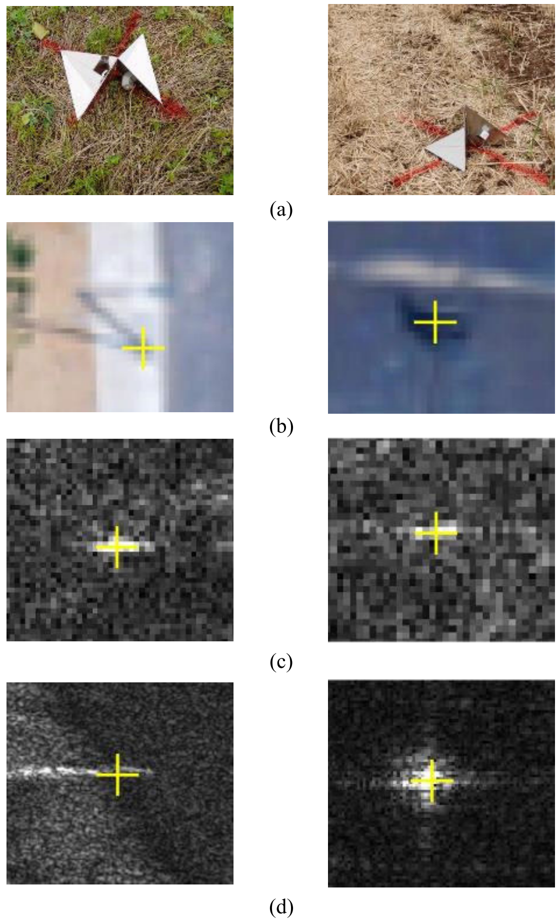

FIGURE 5. Partial control points scenario. (a) Field-deployed corner reflectors. (b) Manually acquired control points in the optical images. (c) Corner reflectors in the SAR images. (d) Manually acquired control points in SAR images.

The distribution of the control points in the experimental area is shown in Fig. 6. There were more control points in the north, central west, and southwest, which mainly comprises open land or artificial structures and were suitable to be

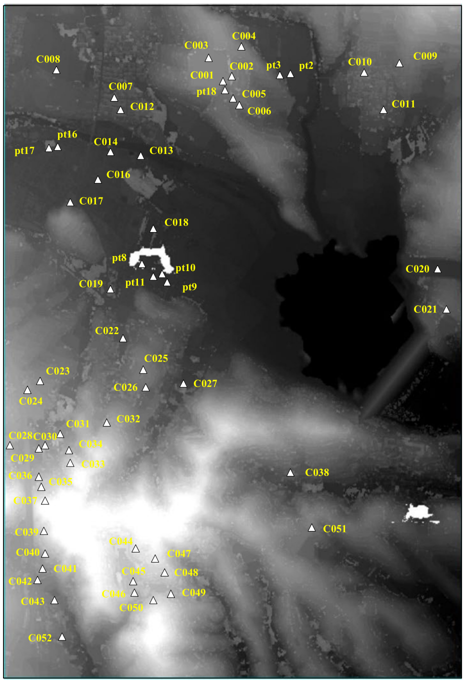

FIGURE 6. **Distribution of control points.**

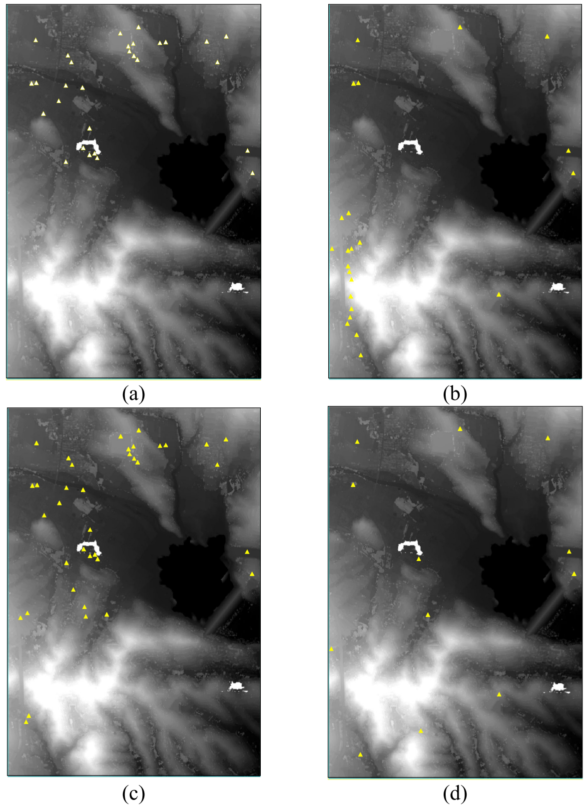

FIGURE 7. **Control point layout plans. (a) Unilateral layout. (b) External layout. (c) Flat area layout. (d) Uniform layout.**

selected as control points. The central east is the reservoir area, and the southeast is an area covered with vegetation, where it is difficult to obtain control points.

The connection points were matched and obtained using the SAR-SIFT algorithm [27]. After decimating, 4652 pairs of connection points were obtained from 28 SAR images. An average of 140 pairs of connection points were extracted for image pairs with 60% overlap, and 10 pairs of connection points were extracted for image pairs with 20% overlap.

B. BLOCK ADJUSTMENT RESULTS

A subset of the control points was selected for adjustment, and the remaining points were used as checkpoints to evaluate the adjustment results. In order to compare the results of the adjustment experiment better, first use the RD model parameters obtained by the UAV and the sensors on the SAR to calculate all the control points and count the residuals. It is calculated that without adjustment, the RMSE of all control points in the three directions are 2.868m, 1.045m and 3.318m respectively, totaling 4.509m. Four control-point layout plans were set up for the experiment (Fig. 7). Fig. 7 (a) shows the unilateral layout, where the selected control points are concentrated in the north of the experimental area and the checkpoints are in the south. This plan is consistent with the direction of the averted vision of the radar from north to south and can simulate the situation when the UAV cannot span the target area. Fig. 7 (b) shows the external layout, where the selected control points are within 200 m from the boundary of the experimental area and point C051 in the southeast corner. The check points are located inside the experimental area. This plan is used to simulate the situation where the inner area is inaccessible. Fig. 7 (c) shows the flat area layout, where the control points are located in the flatter area, and the check points are located in the hilly area with a larger slope. Generally, control points are easier to set up in areas with gentle slopes. This plan was used to simulate the case of inaccessible areas with an undulating terrain. Fig. 7 (d) shows the uniform layout, where the control points are located at the edges, corners, and center of the experimental area. The points were relatively evenly distributed and were few in number. This plan was used to simulate a situation where a small number of control points were used to conduct large-scale topographic surveys.

We conducted separate adjustment calculations using the proposed adjustment method according to the four layout plans. We compared the results with those obtained from the seven- and four-parameter methods. The evaluation indicators of the experiments included the RMSE of the control points and checkpoints, adjustment time, and number of iterations. The RMSE of the control and check points were counted in the adjustment experiment for accuracy assessment. Here, the control point RMSE mainly represents the self-consistency of the algorithm, and the check point RMSE mainly represents the accuracy of the algorithm. In this experiment, the RMSE was divided into the X, Y, and Z directions. Because the flight direction was from west to east, the X, Y, and Z directions corresponded to the range, azimuth,

TABLE 2. Results of adjustment experiments.

Layout plan	Evaluation indicators		Seven-parameter method	Four-parameter method	Proposed method
Unilateral layout Control points: 30 Check points: 31	Control points RMSE (m)	X	1.030	**0.261**	0.342
		Y	0.581	**0.556**	1.077
		Z	1.159	**0.326**	0.729
		Total	1.656	**0.695**	1.344
	Check points RMSE (m)	X	6.160	3.102	**0.374**
		Y	1.671	0.665	**0.508**
		Z	6.501	3.084	**0.354**
		Total	9.110	4.424	**0.723**
	Time (s)		688.2	681.9	**129.195**
	Number of iterations		3000	3000	**690**
External layout Control points: 23 Check points: 38	Control points RMSE (m)	X	0.358	0.369	**0.329**
		Y	**0.299**	0.370	1.672
		Z	0.469	**0.431**	0.797
		Total	**0.661**	0.677	1.881
	Check points RMSE (m)	X	6.645	3.831	**2.980**
		Y	2.649	**0.895**	1.430
		Z	7.375	4.297	**2.792**
		Total	10.274	5.826	**4.327**
	Time (s)		696.3	683.7	**90.2**
	Number of iterations		3000	3000	**475**
Flat area layout Control point: 38 Check points: 23	Control points RMSE (m)	X	0.916	**0.366**	0.458
		Y	0.548	**0.532**	0.994
		Z	1.005	**0.457**	0.757
		Total	1.466	**0.791**	1.331
	Check points RMSE (m)	X	8.777	3.002	**1.414**
		Y	1.491	0.715	**1.132**
		Z	10.029	3.253	**1.581**
		Total	13.410	4.616	**2.404**
	Time (s)		687.6	658.5	**100.8**
	Number of iterations		3000	3000	**533**
Uniform layout Control points: 13 Check points: 48	Control points RMSE (m)	X	**0.399**	0.411	0.585
		Y	**0.225**	0.519	1.767
		Z	**0.399**	0.431	1.188
		Total	**0.607**	0.790	2.208
	Check points RMSE (m)	X	8.430	3.599	**0.680**
		Y	1.528	**0.501**	0.882
		Z	8.954	3.609	**0.725**
		Total	12.392	5.121	**1.329**
	Time (s)		695.5	658.484	**85.312**
	Number of iterations		3000	3000	**446**

and elevation directions, respectively. Adjustment time is the running time of the adjustment calculation program written in C++ language. The configuration of the laptop used for the experiment was as follows: the operating system was Windows 10 21H2 x64, CPU was Intel i9-9880H, and memory size was 64 GB. To consider the account efficiency and accuracy in actual applications, the upper limit of the number of iterations was set to 3000 from experience. The results of the adjustment experiments are listed in Table 2.

The following are the analysis results of the data in Tab. 2:

1. Comparison of the adjustment accuracies of the three adjustment methods. In terms of checkpoints, the proposed method always obtains the optimal value in the X- and Z-directions and in the overall RMSE, achieving the highest accuracy. The four-parameter method had a slightly higher accuracy in the Y-direction, but the overall adjustment accuracy was not as good as that of the proposed method. The seven-parameter method had the lowest overall adjustment accuracy because a certain degree of correlation exists between the orientation parameters selected by the seven- and four-parameter methods. In addition, the initial errors are inclined to compensate for each other in the two directions of the vertical track, that is, the range and vertical directions. This results in an increase in the errors in the X- and Z-directions for these two methods, affecting the accuracy of the adjustment and being not conducive to the convergence of the iterations. The correlation between the orientation parameters selected using the proposed method was weak, and the errors were more evenly distributed in the three directions. Although the accuracy in the Y-direction was slightly lower, the overall adjustment accuracy should be improved. In terms of control points, the seven- and four-parameter methods generally perform better in terms of RMSE than the proposed method, because a larger number of orientation parameters in the adjustment process can better match the control points. However, if we simultaneously refer to the RMSE of the checkpoints, we can identify an "overfitting" phenomenon where it is difficult to match the adjustment results with the checkpoints. Comparing the unadjusted results, it can be seen that the accuracy of the seven-parameter and four-parameter adjustment is worse in some cases. This is because the "overfitting" phenomenon will occur when the number and distribution of control points are not good. Reduced precision for checkpoints not participating in adjustments. However, the proposed method can always achieve higher totaling accuracy. Therefore, the proposed method is better than the seven- and four-parameter methods. Consequently, the proposed method achieved the highest adjustment accuracy.
2. The robustness and efficiency of the three adjustment methods were compared. The proposed method always has the shortest adjustment time and the lowest number of iterations. The four-parameter method requires a longer time, the seven-parameter method required the longest time and both reached the upper limit of the set number of iterations in all the cases. Reaching the set upper limit implies that the convergence condition is not strictly reached in the adjustment process, and the result is a forced output after a certain number of iterations, indicating that the algorithm is less robust. The reason is that the seven- and four-parameter methods choose a large number of orientation parameters with a certain degree of correlation, which is not conducive to the convergence of iterations, affecting the robustness and efficiency of the adjustment. The orientation parameters chosen by the proposed method have a weak correlation and are smaller in number, which is conducive to rapid convergence of the adjustment

iterations. Therefore, the proposed method achieved the highest robustness and adjustment efficiency.

3. In the experiments with different control-point layout plans, the results of the three adjustment methods showed the same pattern. The unilateral layout plan makes full use of the advantage of the averted vision of the SAR; however, the checkpoint accuracy is poorer because the control points are concentrated in the north, making it difficult to effectively control the south. The external layout plan simulates another inaccessible situation for which it is difficult to achieve effective control over a large area at the center. Moreover, because more control points were concentrated in the southeast, which significantly reduced the control in other directions, the overall accuracy was worse than that of the unilateral layout plan. The flat area layout plan used most control points, but the accuracy was unsatisfactory. This is because the control points were located in areas with a gentle slope, whereas the check points were all located in hilly areas with large undulations. Accurate terrain restoration is difficult to achieve using only the connection points in the absence of control points. Therefore, a certain number of control points must be deployed in these areas to obtain high-accuracy adjustment results in hilly areas with large undulations. The uniform layout plan has the least number of control points but always has the best accuracy and highest efficiency. This is because the control points in this plan cover most of the survey area and include different terrains, such as flat land and hills, which can better restore the entire survey area. Thus, when the control points are distributed more evenly in the survey area, only a small number of control points are required to achieve a higher adjustment accuracy. A comparison of the different layout plans showed that the highest adjustment accuracy could be obtained with relatively uniformly distributed control points in the survey area. In addition, the proposed method could still obtain a relatively high adjustment accuracy under three difficult conditions, further confirming the effectiveness of the proposed method.

C. NUMBER OF CONTROL POINTS EXPERIMENT

The results in Section B show that the proposed method can achieve good accuracy when the distribution of control points is uniform. In order to explore the influence of the number of control points on the adjustment results, an experiment on the number of control points was set up, as shown in Fig. 8. The proposed method is used to adjust the number of different control points, and the coordinate residuals of the check points are counted. The results are shown in Fig. 9.

As shown in Fig. 9, the optimal number of control points for this data set was 13, and the geometric model of the adjustment was then not sensitive to control point number. With the increase of control point number, the RMSEs decreased,

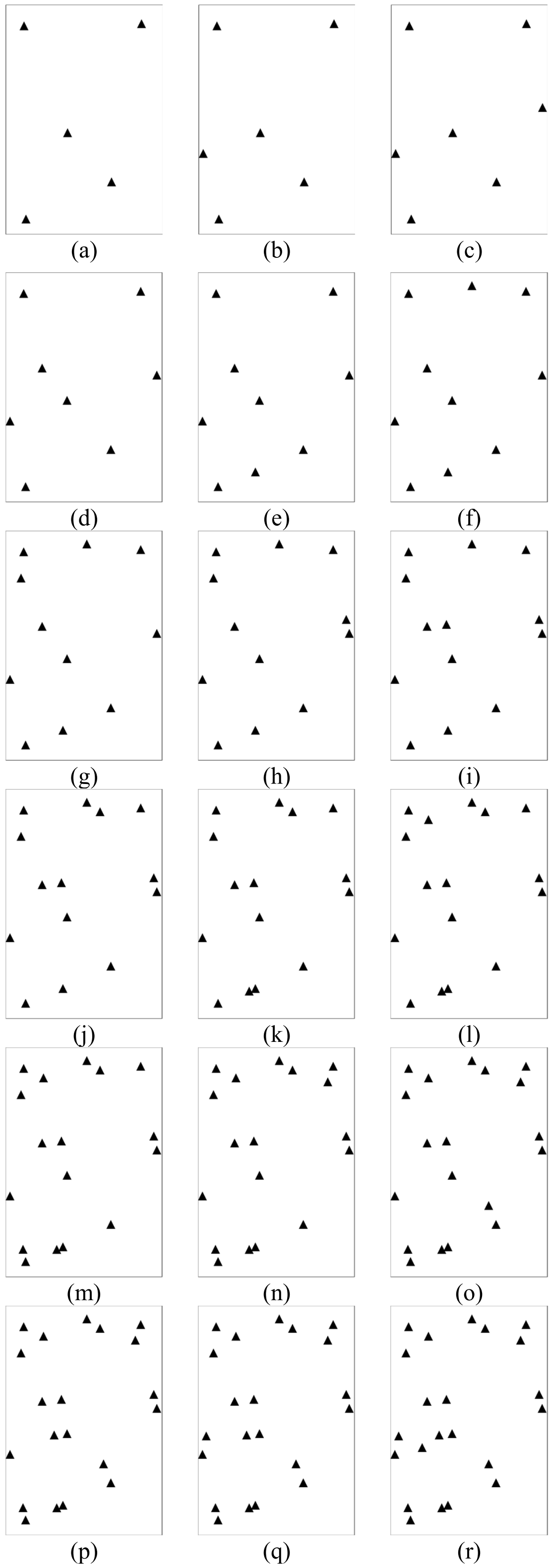

FIGURE 8. Adjustment tests with different control points numbers. (a) to (r) represent the number of control points varying from 5 to 22, respectively.

and achieved a smaller value and remained almost unchanged when the number of control points reached 13. It can be seen that the proposed method can obtain stable accuracy with a

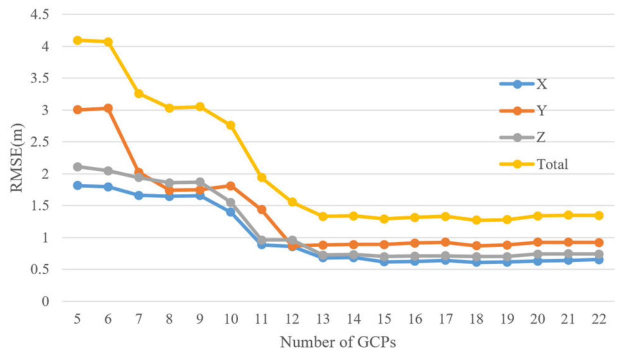

FIGURE 9. RMSE of all 18 tests with different GCP numbers.

small number of 13 control points, which proves the effectiveness of the method for reducing the number of control points.

IV. CONCLUSION

In this paper, we proposed a robust block-adjustment method for UAV SAR images for a UAV SAR system with a small imaging width and poor platform stability. The method was based on the RD model and was designed to solve the three orientation parameters of the antenna phase center initial imaging moment, Doppler centroid, and proximity delay for block adjustment by analyzing the parameter correlation of the seven-orientation parameters. This method considers that the initial position adjustment solution is inclined to compensate for each other in the range and vertical directions. We used UAV SAR images of the Dengfeng area for the adjustment experiments. Subsequently, we compared the adjustment methods with different orientation parameter settings. The proposed method exhibited the highest accuracy and efficiency and was most likely to achieve the conditions for convergence. By comparing the adjustment results of different control-point layout plans, the proposed method achieved an adjustment accuracy better than 1 m with a small number of control points under the condition of a uniform layout plan and had certain practical value in some difficult situations. The robustness and effectiveness of the proposed method were confirmed.

Due to practical limitations, the experimental area was mainly concentrated in flat areas and hills, and experimental verification of this method in areas with highly undulating terrain was limited. Based on experience, the adjustment accuracy of the proposed method will be relatively low in areas with highly undulating terrain; however, the specific value still requires experimental verification. The distribution of control points in the experiment was not ideal, and sparse control points in some areas adversely affected the adjustment solution. However, this issue should be addressed in future studies.

REFERENCES

[1] F. Bovenga, "Special issue 'Synthetic Aperture Radar (SAR) techniques and application,"' *Sensors*, vol. 20, no. 7, p. 1851, Mar. 2020.

[2] F. Xu, Y. Zhang, R. Wang, C. Mi, Y. Zhang, Y. Huang, and J. Yang, "Heuristic path planning method for multistatic UAV-borne SAR imaging system," *IEEE J. Sel. Topics Appl. Earth Observ. Remote Sens.*, vol. 14, pp. 8522–8536, 2021.

[3] J. Zhang, S. Yang, Z. Zhao, and G. Huang, "SAR mapping technology and its application in difficulty terrain area," in *Proc. IEEE Int. Geosci. Remote Sens. Symp.*, Jul. 2010, pp. 3608–3611.

[4] Q. Jiao, W. Jiang, H. Qian, and Q. Li, "Research on characteristics and failure mechanism of Guizhou Shuicheng landslide based on InSAR and UAV data," *Natural Hazards Res.*, vol. 2, no. 1, pp. 17–24, Mar. 2022.

[5] J. Wasowski and F. Bovenga, "Remote sensing of landslide motion with emphasis on satellite multi-temporal interferometry applications: An overview," in *Landslide Hazards, Risks, and Disasters*, T. Davies, N. Rosser, and J. F. Shroder, Eds., 2nd ed. Amsterdam, The Netherlands: Elsevier, 2022, ch. 11, pp. 365–438.

[6] A. M. Lechner, G. M. Foody, and D. S. Boyd, "Applications in remote sensing to forest ecology and management," *One Earth*, vol. 2, no. 5, pp. 405–412, May 2020.

[7] X. Xiong, G. Jin, Q. Xu, and H. Zhang, "Block adjustment with airbrone SAR very high-resolution images using trajectory constraints," *Int. J. Remote Sens.*, vol. 39, no. 8, pp. 2383–2398, Apr. 2018.

[8] J. C. Curlander, "Location of spaceborne SAR imagery," *IEEE Trans. Geosci. Remote Sens.*, vol. GRS-20, no. 3, pp. 359–364, Jul. 1982.

[9] C. Cheng, J. Zhang, K. Deng, and L. Zhang, "Range-coplanarity equation for radar geometric imaging," *J. Remote Sens.*, vol. 16, no. 1, pp. 38–49, 2012.

[10] G. Konecny and W. Schuhr, "Reliability of radar image data," *Int. Arch. Photogramm. Remote Sens.*, vol. 27, pp. 456–469, Jul. 1988.

[11] C. V. Tao and Y. Hu, "A comprehensive study of the rational function model for photogrammetric processing," *Photogramm. Eng. Remote Sens.*, vol. 67, no. 12, pp. 1347–1358, 2001.

[12] F. W. Leberl, *Radargrammetric Image Processing*. Norwood, MA, USA: Artech House, 1990.

[13] X. J. Yue, G. M. Huang, Y. Zhang, Z. Zhang, and L. Pang, "Multi-photo combined adjustment with airborne SAR images based on F. Leberl orthorectific model," *Int. Arch. Photogramm., Remote Sens. Spatial Inf. Sci.*, vol. 37, pp. 357–360, Jun. 2008.

[14] G. Zhang, W.-B. Fei, Z. Li, X. Zhu, and D.-R. Li, "Evaluation of the RPC model for spaceborne SAR imagery," *Photogramm. Eng. Remote Sens.*, vol. 76, no. 6, pp. 727–733, 2010.

[15] N. Jiao, F. Wang, H. You, X. Qiu, and M. Yang, "Geo-positioning accuracy improvement of multi-mode GF-3 satellite SAR imagery based on error sources analysis," *Sensors*, vol. 18, no. 7, p. 2333, 2018.

[16] J. Zhang, C. Cheng, and G. Huang, "Block adjustment of POS-supported airborne SAR images," in *Proc. 12th Int. Radar Symp. (IRS)*, Leipzig, Germany, 2011, pp. 863–868.

[17] N. Jiao, F. Wang, H. You, and X. Qiu, "Geolocation accuracy improvement of multiobserved GF-3 spaceborne SAR imagery," *IEEE Geosci. Remote Sens. Lett.*, vol. 17, no. 10, pp. 1747–1751, Oct. 2020.

[18] S. C. Yang, G. M. Huang, Z. Zhao, and L. J. Lu, "Method of airborne SAR image match integrating multi-information for block adjustment," *Int. Arch. Photogramm., Remote Sens. Spatial Inf. Sci.*, vol. 40, pp. 191–195, Jun. 2015.

[19] T. Toutin and K. Omari, "A 'new hybri' modeling for geometric processing of Radarsat-2 data without user's GCP," *Photogramm. Eng. emote Sens.*, vol. 77, no. 6, pp. 601–608, Jun. 2011.

[20] Z.-W. Huang and S. He, "A method for improving positioning accuracy of SAR imagery based on RFM," in *Proc. 4th Int. Conf. Digit. Manuf. Autom.*, Shinan, China, Jun. 2013, pp. 43–46.

[21] G. Zhang, Q. Wu, T. Wang, R. Zhao, M. Deng, and B. Jiang, "Block adjustment without GCPS for Chinese spaceborne SAR GF-3 imagery," *Sensors*, vol. 18, no. 11, p. 4023, 2018.

[22] N. Jiao, F. Wang, and H. You, "A new combined adjustment model for geolocation accuracy improvement of multiple sources optical and SAR imagery," *Remote Sens.*, vol. 13, no. 3, p. 491, 2021.

[23] Y. Xiang, F. Wang, and H. You, "OS-SIFT: A robust SIFT-like algorithm for high-resolution optical-to-SAR image registration in suburban areas," *IEEE Trans. Geosci. Remote Sens.*, vol. 56, no. 8, pp. 3078–3090, Jun. 2018.

[24] J. C. Curlander and R. N. McDonough, *Synthetic Aperture Radar*. New York, NY, USA: Wiley, 1991.

[25] H. Johnsen, L. Lauknes, and T. Guneriussen, "Geocoding of fast-delivery ERS-L SAR image mode product using DEM data," *Int. J. Remote Sens.*, vol. 16, no. 11, pp. 1957–1968, Jul. 1995.
[26] Z. Hong-Min, J. Guo-Wang, X. Qing, and L. Xiangying, "Accurate positioning with stereo SAR images and one ground control point," *J. Radars*, vol. 3, no. 1, pp. 85–91, 2014.
[27] F. Dellinger, J. Delon, Y. Gousseau, J. Michel, and F. Tupin, "SAR-SIFT: A SIFT-like algorithm for SAR images," *IEEE Trans. Geosci. Remote Sens.*, vol. 53, no. 1, pp. 453–466, Jan. 2015.

YUNHAO CHANG was born in Luohe, Henan, China, in 1991. He received the B.S. and M.S. degrees in photogrammetry and remote sensing from Southwest Jiaotong University, Chengdu, Sichuan, China, in 2012 and 2015, respectively. He is currently pursuing the Ph.D. degree with Information Engineering University, Zhengzhou, China.

He is also an Assistant Professor with the Henan College of Surveying and Mapping. His research interests include radargrammetry and UAV remote sensing.

QING XU received the B.S., M.S., and Ph.D. degrees in photogrammetry and remote sensing from the Institute of Geospatial Information, Information Engineering University, Zhengzhou, China, in 1985, 1990, and 1995, respectively.

He is currently a Professor and a Doctoral Supervisor with Information Engineering University. His research interests include photogrammetry and deep space remote sensing mapping.

Dr. Xu has been a member of the Professional Committee of the *Photogrammetry and Remote Sensing* of the Chinese Society for Geodesy, Photogrammetry and Cartography (CSGPC), since 2000. Since 2004, he has been a member of the Professional Committee of the Deep Space Exploration of the Chinese Society of Astronautics (CSA). Since 2006, he has been a member of the Expert Committee of the Scientific Application of the Exploring Project around the Moon.

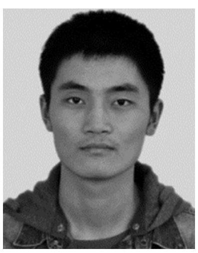

XIN XIONG received the B.S., M.S., and Ph.D. degrees in photogrammetry and remote sensing from the Institute of Geospatial Information, Information Engineering University, Zhengzhou, China, in 2014, 2017, and 2021, respectively.

He is currently a Lecturer with Information Engineering University. His research interests include image feature extraction and matching.

GUOWANG JIN received the B.S., M.S., and Ph.D. degrees in photogrammetry and remote sensing from the Institute of Geospatial Information, Information Engineering University, Zhengzhou, China, in 2000, 2003, and 2007, respectively.

He is currently a Professor and a Doctoral Supervisor with Information Engineering University. His research interests include radargrammetry and synthetic aperture radar (SAR) interferometry.

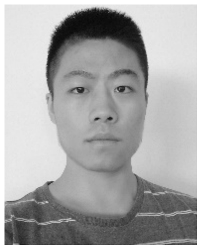

HUITAI HOU received the B.S. degree in photogrammetry and remote sensing from the Zhengzhou Institute of Surveying and Mapping, China, in 2018. He is currently pursuing the Ph.D. degree in surveying and mapping with the Institute of Geospatial Information, Information Engineering University.

His research interests include photogrammetry and UAV remote sensing.

RUIBING CUI received the B.S. degree in geomatics engineering from the North China University of Water Resources and Electric Power, Zhengzhou, China, in 2013, and the M.S. degree in photogrammetry and remote sensing from Information Engineering University, Zhengzhou, in 2016, where he is currently pursuing the Ph.D. degree.

He is also an Assistant Professor with the Henan College of Surveying and Mapping. His research interest includes the registration of multi-source remote sensing image.